Earth and Planetary Science Letters 558 (2021) 116760

Contents lists available at ScienceDirect

Earth and Planetary Science Letters

www.elsevier.com/locate/epsl

First evidence of eclogites overprinted by ultrahigh temperature metamorphism in Everest East, Himalaya: Implications for collisional tectonics on early Earth

Jia-Min Wang [a,*], Pierre Lanari [b], Fu-Yuan Wu [a], Jin-Jiang Zhang [c], Gautam Prashad Khanal [a,d], Lei Yang [a,d]

[a] State Key Laboratory of Lithospheric Evolution, Institute of Geology and Geophysics, Chinese Academy of Sciences, 100029 Beijing, China
[b] Institute of Geological Sciences, University of Bern, 3012 Bern, Switzerland
[c] School of Earth and Space Sciences, Peking University, 100871 Beijing, China
[d] College of Earth and Planetary Sciences, University of Chinese Academy of Sciences, Beijing 100029, China

ARTICLE INFO

Article history:
Received 26 July 2020
Received in revised form 25 December 2020
Accepted 11 January 2021
Available online xxxx
Editor: A. Webb

Keywords:
modern-style plate tectonics
continental collision
Himalaya
eclogite
ultrahigh temperature
crustal thickening

ABSTRACT

Modern-style plate tectonics, often characterised by subduction, is a fundamental dynamic process for planet Earth. Subduction related eclogites are widely used to indicate initiation of plate tectonics or whether different tectonic regimes dominated Earth history. However, such markers are commonly overprinted in ancient metamorphic terranes and rarely preserved even in most Phanerozoic mountain belts. This study tries to reveal the detailed burial and exhumation processes that formed granulitized eclogites in the Everest east region, central Himalaya, so as to explore the tectonic regimes recorded by similar rocks on early Earth. Robust Pressure-Temperature-time paths were achieved by studying the mineral relicts (Omp, Jd ~29%), high-temperature mineral textures (Sil-Crd-Qz-Spl-Mesoperthite assemblage, rutile exsolution in biotite), and multiple thermobarometry and petrochronology of eclogites and metapelites. Results show that these eclogites underwent eclogitization at conditions of 730–770 °C and ~20 kbar (~11 °C/km) at ~30 Ma and were overprinted by a heating and decompression path to ultrahigh temperature (UHT) conditions of 6–11 kbar and 900–970 °C (~40 °C/km) during 25–15 Ma. The resulting exhumation rate (2–3 mm/yr) is slow and prolonged (10–15 Myr) (U)HT favoured re-equilibration of the eclogitic mineral assemblage and textures. The obtained UHT conditions, the first time ever reported for the Himalaya, were induced by combined effects of over-thickened (~60 km) radioactive felsic crust and thinning of lithosphere to <90 km. This case study provides a critical example to understand the heat sources and timescale of UHT condition during continental collision. By comparing with the western Himalaya eclogites, we suggest that formation of cold vs. granulitized continental eclogites during the Himalayan orogeny is caused by different crustal thickness (normal ~30 km vs. over-thickened ~60 km) due to different collisional stages (infant vs. mature). In a wider perspective, ancient eclogites were commonly granulitized by stacking into the over-thickened orogenic crust during mature continental collision. According to similar granulitized eclogites preserved on early Earth, Himalaya-type continental subduction/collision should have become a global pattern during the Paleoproterozoic (2.0–1.8 Ga).

1. Introduction

The surface dynamics of planet Earth is characterised by plate tectonics as the Earth's lithosphere is composed of a mosaic of plates that move along convergent, divergent or transform boundaries. Plate tectonics drives fundamental processes such as growth of continental crust, topography and it controls the main mass transfers between the Earth's crust and mantle (Condie and Kröner, 2008). Therefore, one of the main tasks in geoscience is to explore when modern-style plate tectonics—characterised by cold subduction—started on Earth and to understand what plate tectonic regimes dominated through Earth's history.

The thermal regime recorded in metamorphic rocks is a good indicator for styles of plate tectonics (Brown, 2006), as cold geotherms are characteristic of oceanic and continental subduction. Eclogites or blueschists that underwent cold HP metamorphism

* Corresponding author.
E-mail address: wangjiamin@mail.iggcas.ac.cn (J.-M. Wang).

https://doi.org/10.1016/j.epsl.2021.116760
0012-821X/

have been a key target to explore initiation of modern-style plate tectonics on Earth. Unfortunately, such rocks are rarely preserved and commonly overprinted across ancient metamorphic terranes. Cold eclogites/blueschists that definitely indicate subduction tectonics (thermal gradients of 5–10 °C/km or 350 °C/Gpa) are mostly present during the Phanerozoic or after 0.75 Ga (Brown, 2006). A few studies reported high-pressure eclogites back to the Paleoproterozoic (2.0∼1.8 Ga, e.g. Möller et al., 1995; Mints et al., 2010; Weller and St-Onge, 2017; Xu et al., 2018) or high-pressure garnet-amphibole of mid-Archaean age (Moyen et al., 2006). Although the authors argue for a (cold) subduction in the ancient Earth, most of these high-pressure rocks are different from the indicative cold eclogite/blueschist in intense high-temperature overprinting and are characterised by an intermediate thermal gradient of 10–15 °C/km at pressure peak. Meanwhile, most ancient metamorphic terranes are filled with abundant medium-pressure granulite-facies and a small number of high-pressure granulite-facies metamorphic rocks (>15 °C/km, such as the 1.9∼1.8 Ga Chinese Hengshan, Zhao et al., 2001), which could have formed during diverse tectonic settings and are not conclusive of modern-style plate tectonics. Even in the Phanerozoic collisional belts, high-pressure granulite-facies rocks are abundant and occasionally preserve eclogite-facies relicts (such as the Variscan Bohemian Massif, O'Brien et al., 1992), whereas cold eclogites occupy only less than 1 vol% of the total area or are even absent.

This invokes several fundamental questions. Why are eclogites from ancient to modern mountain belts commonly overprinted by granulite-facies metamorphism? Are the oldest eclogites on Earth indicative of modern-style plate tectonics? Why no eclogite was preserved in Archean metamorphic terranes despite that arc-type magmatism and isotopic evidences of recycled superficial material suggest that modern-style plate tectonic was ongoing at 2.7–2.5 Ga (Condie and Kröner, 2008)? Answering these questions is crucial for our understanding of early plate tectonics on Earth, but answers cannot be obtained unless burial and exhumation processes of similar eclogites are dissected from a recent and better preserved mountain belt.

The Himalaya is a typical example of modern-style plate tectonics due to its well-understood crustal architectures and collisional processes. The Himalaya is beneficial in that two contrasting eclogite types (cold vs granulitized) are present for comparison (e.g. Lombardo and Rolfo, 2000; Guillot et al., 2008). In the western Himalayan syntax, (ultra)high pressure eclogites that indicate cold continental subduction (∼7 °C/km) are preserved, whose P-T-time evolution has been clearly depicted (O'Brien et al., 2001; Lanari et al., 2013). However, in the central Himalaya, the burial and exhumation processes leading to the formation of granulitized eclogites (Lombardo and Rolfo, 2000; Groppo et al., 2007) are still debated due to controversy in the P-T evolution and timing of eclogitization and granulitization (e.g. Kellett et al., 2014; Wang et al., 2017a). Therefore, resolving the mystery of why some eclogites were relatively well preserved whereas others were heavily granulitized within the same collisional belt is key to better constrain deep collisional tectonics and potentially to imply tectonic regimes recorded by similar eclogites from the early Earth. In this contribution, we retrieved the P-T-time evolution of granulitized eclogite from Everest East region in a high degree of details by the mean of comprehensive petrography, thermobarometric and petrochronologic investigations, and then we compare the result to the well-studied western Himalayan eclogites. A new model that conforms to present geophysical observations in the Himalaya is proposed to reconcile these new finding and may shed light on a better understanding of early Earth tectonic regimes.

2. Geological setting

The Himalayan orogen is commonly divided into the Tethyan Himalayan Sequence, Greater Himalayan Crystalline complex (GHC), Lesser Himalayan Sequence and Siwalik Group (Fig. 1a), which are separated by the South Tibetan Detachment (STD), Main Central Thrust (MCT), Main Boundary Thrust and Main Frontier Thrust from north to south. Within these sequences, the GHC represents the metamorphic core and is mainly composed of amphibolite- to granulite-facies metasedimentary rocks, Early Paleozoic orthogneiss and Oligocene–Miocene leucogranite (e.g., Le Fort, 1986). Exhumation of the GHC is commonly suggested to be assisted by coeval movement along the STD and MCT during early to mid-Miocene (e.g., Burchfiel et al., 1992).

The Everest east region is located in south Tibet, central Himalaya (Fig. 1b). Main lithotectonic units in this region include the THS, GHC and Ama Drime Massif (ADM). Foliations of the GHC dip to the north or northwest at moderate angles (20°–50°) and lineations in the STD shear zone plunge to the northeast at 5°–30°. The migmatitic paragneiss recorded the highest metamorphic grade within the kyanite-bearing field, and underwent decompression into sillimanite-grade and finally to cordierite-spinel bearing field (Wang et al., 2017b). The ADM presents an east–west extensional domal structure, which was caused by orogen-parallel extension and offset along the Xainza-Dinggye rift. The ADM has an affinity with the LHS that is mainly composed of Paleoproterozoic orthogneisses, but the metamorphic grade is similar to what is observed in the GHC. Abundant eclogite lenses are preserved within the ADM (Lombardo and Rolfo, 2000) and GHC (Li et al., 2019), which were overprinted by high-temperature granulite-facies metamorphism (Groppo et al., 2007). The metamorphic conditions at eclogite-facies pressure-peak and granulite-facies overprinting are not well defined. Garnet Lu–Hf dating in the eclogites gives an age of 38–34 Ma (Kellett et al., 2014), whereas zircons yield U–Pb ages of ∼14 Ma (Wang et al., 2017a).

3. Sample description and petrography

Eclogite lenses and their country rocks (migmatitic paragneiss) were collected from the Everest east, south Tibet (Fig. 1b). Sample locations, mineral assemblages, P-T estimates and U-Th-Pb ages are summarized in Appendix C.1. Mineral abbreviations follow Whitney and Evans (2010).

3.1. Eclogite

Numerous eclogite lenses are enclosed by migmatitic paragneiss in the GHC (Fig. 2a–c). The lenses are mostly decimetre to meter-scale in diameter. The eclogites were interpreted to be in situ within the host paragneiss because they underwent similar metamorphic grade during Cenozoic, and no mantle slices were found (O'Brien, 2018). Even the central portion of the lenses is heavily retrogressed and the degree of retrogression increases toward the rim. Some of the eclogite lenses present a bedded structure parallel to the foliation of the migmatitic paragneiss. One eclogite lense is cut by a two-mica leucogranite vein, which was emplaced at ca. 16 Ma (Wang et al., 2017b).

The collected eclogite samples show similar mineral assemblages and textures to the eclogites from Variscan Bohemian Massif (O'Brien et al., 1992) or Paleoproterozoic Belomorian (Mints et al., 2010). The matrix minerals underwent heavy overprinting. Three main stages of mineral equilibration are recognized (Fig. 2d–h). (**i**) The peak-pressure minerals (M1) are preserved as omphacite inclusions in garnet with Jd component values up to ∼29% and Na# (Na/(Na+Ca)) values up to ∼0.36 (Fig. 2d, Fig. 3); Most matrix omphacite has broken down into clinopyroxene + sodic plagioclase forming fine intergrowths characteristic of symplectite

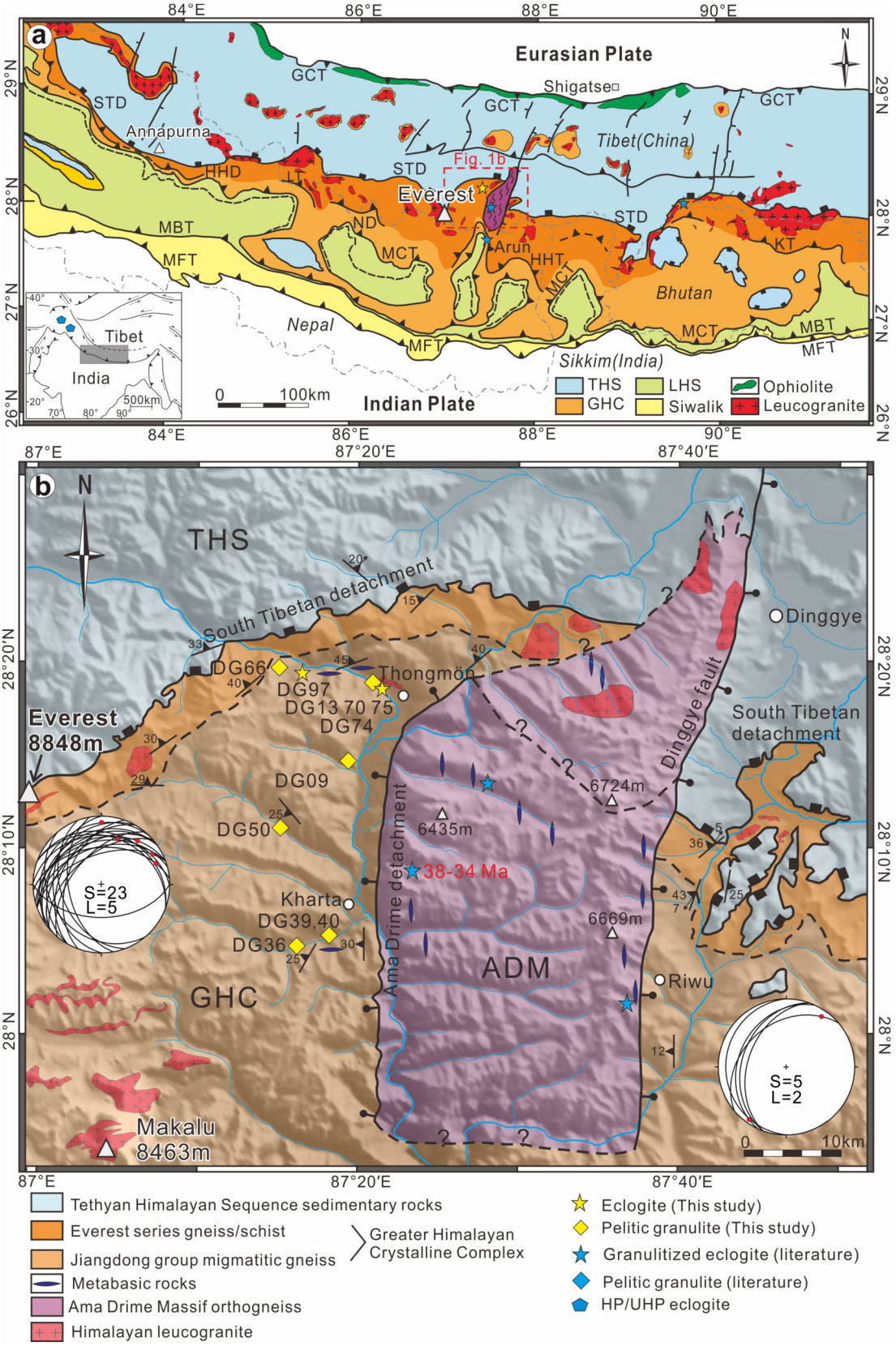

Fig. 1. Geological map of the central Himalaya (**a**) and Everest east region (**b**) (modified after Wang et al., 2017b). GCT, Greater Counter Thrust; STD, South Tibetan Detachment; MCT, Main Central Thrust; MBT, Main Boundary Thrust; MFT, Main Frontier Thrust; HHD, High Himalayan Discontinuity; HHT, High Himalayan Thrust. 38–34 Ma: Kellett et al. (2014). Projection: S, foliation; L, lineation.

(Fig. 2e–h). This reaction was further confirmed by recovering the former omphacite compositions using quantitative compositional maps obtained by electron probe micro-analysis (Fig. 3). The recovered sodic clinopyroxene compositions have a B-site Na content

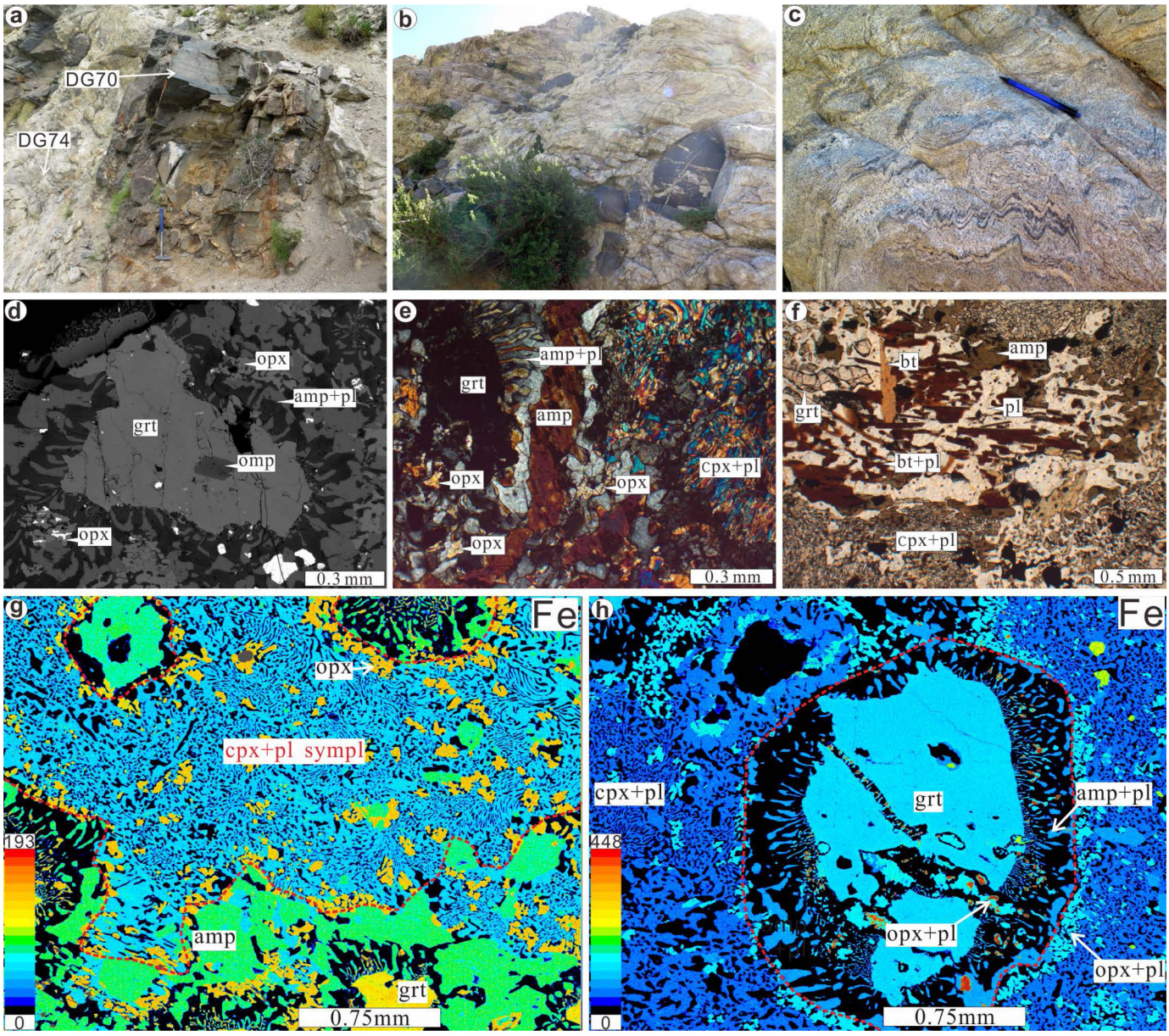

Fig. 2. Outcrop, photomicrographs and X-ray maps (warmer colour indicates higher intensity) of granulitized eclogite from the Greater Himalayan Crystalline Complex (GHC) of Everest east region. **a-c**) Eclogite embedded in migmatitic paragneiss as lens. Significant amount of leucosome is observed in the migmatites (>50 vol%). **d**) Omphacite inclusion within a garnet porphyroblast, showing evidence of retrogression at the rim. **e**) Clinopyroxene + plagioclase symplectite and garnet retrogression into orthopyroxene + plagioclase and amphibole + plagioclase symplectite. **f**) A rare biotite + plagioclase symplectite crystallizes in local domain and was further crosscut by a secondary biotite strip. **g**) Clinopyroxene + plagioclase symplectite by breakdown of omphacite. **h**) Orthopyroxene + plagioclase and amphibole + plagioclase symplectites as corona of a relict garnet. Mineral abbreviations are according to Whitney and Evans (2010). (For interpretation of the colours in the figure(s), the reader is referred to the web version of this article.)

of 0.17–0.23 apfu and A-site Al content of 0.26–0.33. If calculated from the A-site Al compositions as Na can be mobile during symplectite formation, the recovered sodic clinopyroxene should have an average jadeite component value as high as 26–33%, consistent with the omphacite inclusions with the highest Na-content observed in the garnet porphyroblasts. This indicates that the retrogressed matrix clinopyroxene and plagioclase symplectites result from the breakdown of a former omphacite that formed near the pressure peak conditions. (**ii**) Minerals at the high-pressure granulite-facies stage (M2) mainly include the Cpx+Pl symplectite (Fig. 2g,h). Rare biotite + plagioclase symplectites crystallize in local domain (Fig. 2f), which was commonly suggested to form by breakdown of phengite when observed in eclogite (Groppo et al., 2007 and reference therein). The symplectite was further crosscut by a secondary biotite strip, suggesting that some biotite may crystallize from melt during retrograde cooling. (**iii**) Orthopyroxene + calcic plagioclase symplectites developed at the rim of garnet or clinopyroxene (Fig. 2e,h), characterising the medium- to low-pressure and high-temperature overprinting stage (M3). The equilibrated mineral assemblage at the M3 stage is cpx, opx, pl, ilm, ±grt. Biotite was not interpreted to be in equilibrium with the M3-stage minerals because it occurs outside the reaction domain (Fig. 2g,h). (**iv**) hornblende + sodic plagioclase symplectites or hornblende bands form by breakdown of garnet porphyroblast rims or orthopyroxene (Fig. 2g,h), which define the mineral assemblage of the final retrograde stage (M4).

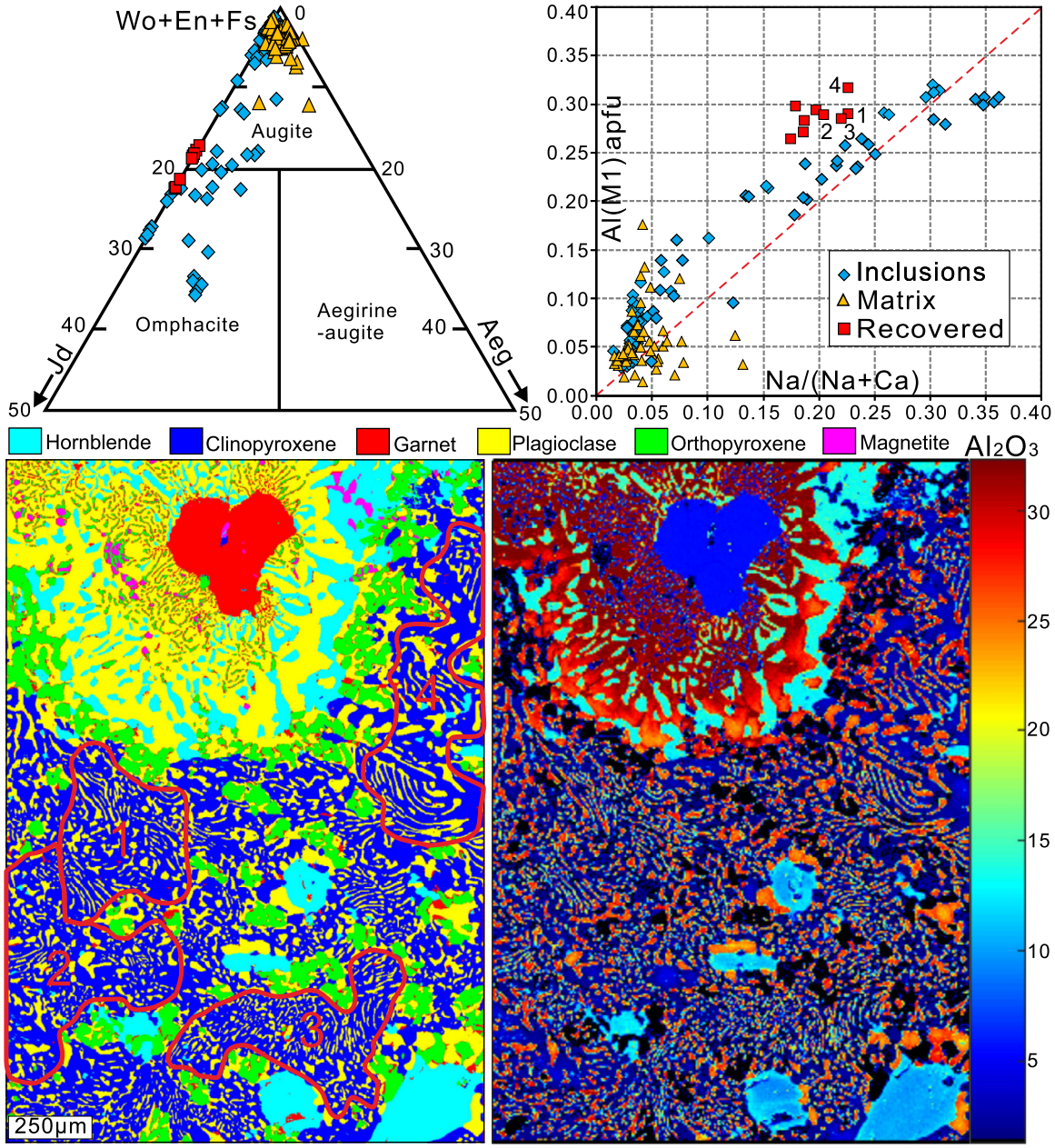

Fig. 3. Mineral phase map of overprinting textures and compositions of omphacite/clinopyroxene in granulitized eclogites. Mineral phases and Al_2O_3 (wt%) maps were processed using the software XMapTools (Lanari et al., 2014) based on merged oxide weight percentage maps; compositions were obtained by applying a density correction (Lanari et al., 2014). The Cpx-Pl symplectite domains resembling an original crystal without involving Opx or Amph are selected for recovering omphacite compositions.

3.2. Migmatitic paragneiss

The migmatitic paragneiss in the country rock underwent distributed partial melting with numerous leucosomes interlayered with biotite-sillimanite bands. Most outcrops contain 20–30 vol% of leucosome, which crystallized as in-situ pores. Leucosomes form strings of discrete lenses or migrated to form parallelling segregations (Fig. 4a). In some outcrops, the parallelling leucosome layers constitute a volume of over 50 vol% (Fig. 4b). The migmatitic metapelites record mineral assemblages from various metamorphic stages. Kyanite and rutile occasionally occur as relict matrix grains or large crystals within the leucosome bands (Fig. 4c), comparable at least to the high-pressure M_2 stage of the eclogite. Most migmatitic metapelites are composed of an inferred equilibrium mineral assemblage of garnet, sillimanite, cordierite, spinel, biotite, plagioclase, K-feldspar, perthite/mesoperthite, quartz and ilmenite, comparable with the M3 stage of the eclogite. Common petrographic phenomena during the M3 stage include: Cordierite + spinel symplectites formed by consumption of garnet (Fig. 4d,e); Cordierite + quartz symplectites formed by consumption of biotite (Fig. 4f); Some spinel grains are enclosed within the Crd-Qz symplectites and have significantly lower Zn (0.6 wt%) and Cr_2O_3 (0.02–0.04 wt%) contents (Fig. 6a); Most biotite grains have been heavily dehydrated and some contain three sets of rutile exsolution (Fig. 4g); In some samples, K-feldspar exist as perthite or mesoperthite (Fig. 4h), where plagioclase lamellae are 5–30 μm thick; In a metapsammite sample, abundant orthopyroxene + calcic plagioclase symplectites were formed by consuming garnet (Fig. 4i).

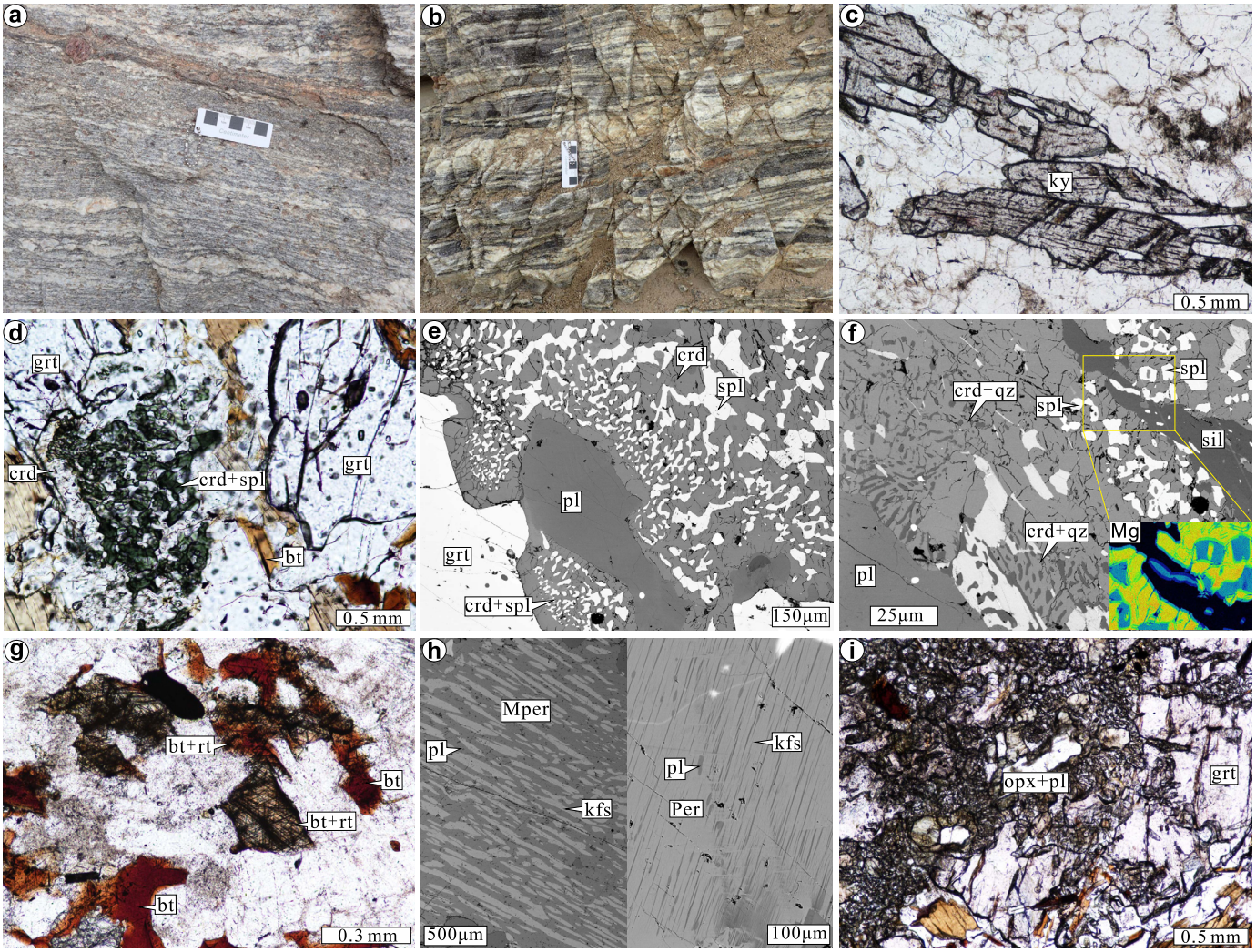

Fig. 4. Outcrop and photomicrographs of migmatitic paragneiss from the GHC of Everest east region. **a-b**) Outcrop of migmatites with extensive parallelling leucosome. **c**) Kyanite relict within leucosome domain. **d,e**) Cordierite + quartz symplectite as corona of garnet. **f**) Spinel in equilibrium with cordierite + quartz symplectite; the elemental map of Mg (insert) shows intergrowth of spinel, cordierite and sillimanite. **g**) Three sets of rutile exsolution in biotite. **h**) In a mesoperthite, K-feldspar lamellae are 30–60 µm thick and occupy around half of the area; in a perthite, plagioclase lamellae are 5–10 µm thick within the K-feldspar host. **i**) Orthopyroxene + calcic plagioclase symplectite within a paragneiss.

4. Thermobarometry

4.1. Phase equilibria modelling

Isochemical phase diagrams (Fig. 5) were calculated using Perplex 6.7.8 (versions June 6th 2017, Connolly, 2009) and the internally consistent thermodynamic dataset of TC-DS622 (Holland and Powell, 2011) based on the XRF-measured bulk composition in the system NCKFMASHTO. Mineral activity–composition solutions are listed in Appendix A, where updated mineral solution models such as tonalitic melt were used to give more reliable estimates compared to previous studies. The modelled mineral assemblages for the eclogite suggest that epidote was absent from the pressure-peak (M1-stage) whereas omphacite was present. Compositional isopleths of omphacite inclusions and recovered omphacite (Jd 29–33% as indicated by Jd components and Al in A-site, Fig. 3) cross the epidote-out field at pressure conditions of ~20 kbar. The calculated Zr-in-Rutile temperatures of samples 15DG70 and 15DG75 (Zr 220–660 ppm) cross the Ep-out and Omph-bearing range and intersect at 730–770 °C with the Jd 29–33% range (Fig. 5b). Rutile grew at high-pressure conditions and did not re-equilibrate to the M3 conditions—the rock only underwent partial re-equilibration involving mostly omphacite breakdown. Therefore, rutile survived (i.e. was not re-equilibrated into ilmenite) and did not exchange Zr during late overprinting. Conservatively, the P-T condition at the M1-stage of 730–770 °C and ~20 kbar (11±1.5 °C/km) are proposed. The predicted mineral assemblage at pressure-peak is garnet, phengite, omphacite, quartz and rutile.

To obtain the P-T condition of the M3 stage, the inferred mineral assemblage of the M3-stage (aug, opx, pl, ilm, L, ±grt) was used in combination with the plagioclase composition in Opx-Pl symplectite that has the highest X_{An} values (>0.85), which indicates P-T conditions of <8 kbar and 900–930 °C (Fig. 5b). Interception of the plagioclase compositional isopleths at the inferred M3-stage mineral assemblage suggests that Ca in plagioclase is a powerful tool to define UHT conditions. Garnet rim compositions (X_{prp} ~0.28) were re-equilibrated by diffusion at high-temperature and indicate medium-pressure granulite-facies conditions. They did not cross the inferred peak-stage mineral assemblage probably because the reaction to form Opx+Pl symplectite by consuming garnet occurred within local domains, which is not compatible with the chosen bulk composition. This result supports that these developed via domanial equilibration, a process that cannot be modelled

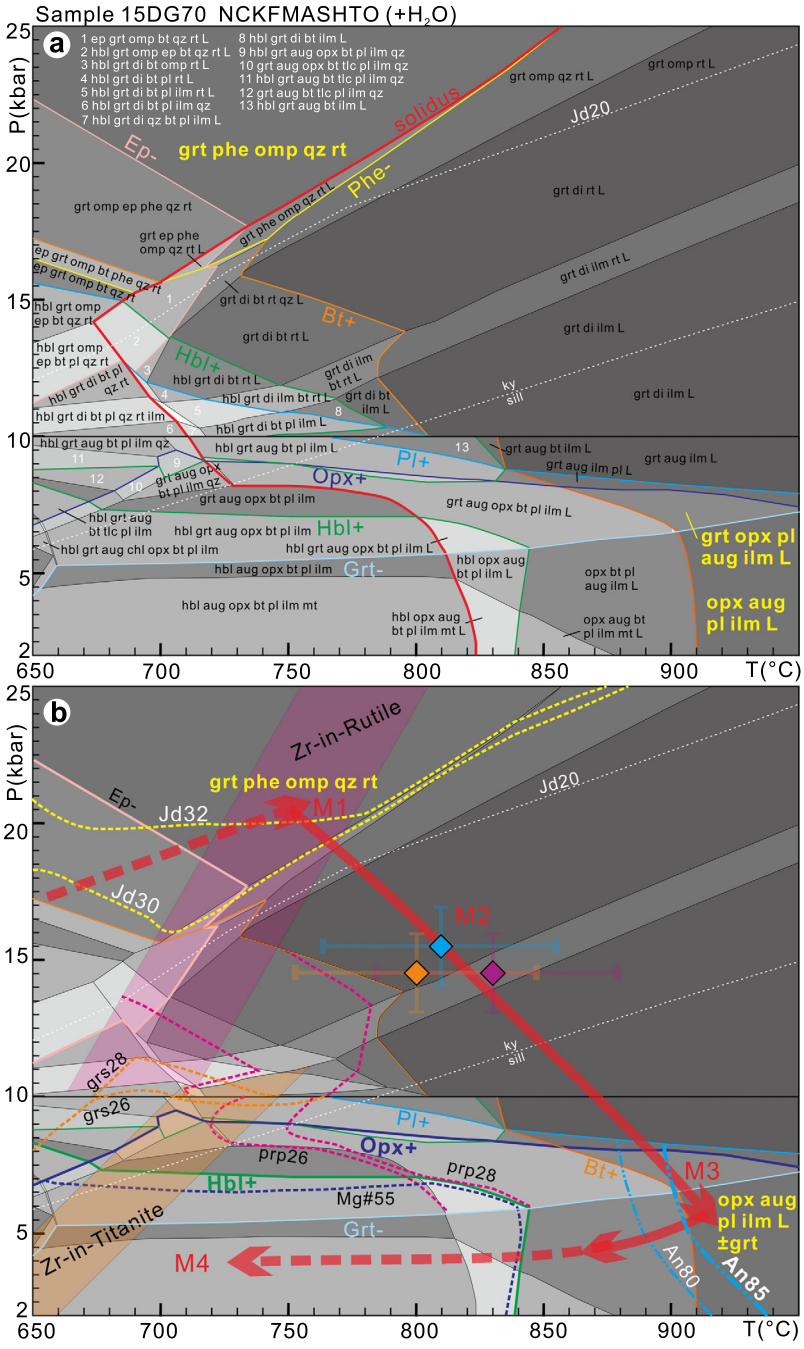

Fig. 5. Phase relationships (**a**) and resulting pressure-temperature path (**b**) of eclogite sample 15DG70. Phase diagrams were calculated using the XRF-measured bulk composition of SiO_2(47.92), TiO_2(1.55), Al_2O_3(15.237), FeO(13.90), MgO(7.18), CaO(11.1), Na_2O(2.13), K_2O(0.42), Fe_2O_3(0.294) (NCKFMASHTO). Omphacitic pyroxene (Di) and augite (Aug) were used for labelling in the high-pressure field (>10 kbar) and medium- to low-pressure fields (<10 kbar), respectively, and the omphacitic pyroxene with a jadeite component larger than 20% was marked as omphacite (Omp). Detailed methods and calibrations used for Zr-in-rutile and Zr-in-titanite temperatures calculations were listed in Appendix A. P-T conditions for the M2 stage are from Grt-Cpx-Pl-Qz thermobarometer with empirical errors of ±1.5 kbar and ±50 °C.

using isochemical phase diagrams based on the bulk composition. The equilibrated P-T conditions of the M4 stage was constrained by the Hbl-in curve and Zr-in-titanite temperatures (Zr 60–140 ppm) to be <7 kbar and <700 °C (Fig. 5b).

4.2. Conventional thermobarometry

For eclogites, the Grt-Cpx-Pl-Qz thermobarometer (Eckert et al., 1991) was used to calculate the P-T conditions of the M2 stage, by using a fixed garnet core composition with the highest X_{grs} values, an average composition of plagioclase and clinopyroxene occurring in the symplectite. The calculated P-T results are mostly distributed around 790–830 °C (±50 °C) for pressures of 16–14 kbar (±1.5 kbar, Fig. 5b). The Grt-Opx-Pl-Qz thermobarometer (Lal, 2010) was used to calculate the P-T conditions of the M3 stage by using the Opx-Pl symplectite compositions and garnet rim (15DG70, 19DG13) or mantle (15DG75) compositions with the lowest Fe# values. Most results are consistently at conditions of 8–10 kbar and 900–940 °C (Fig. 6b), whereas sample 15DG70 indicates slightly higher temperatures of 970–1000 °C.

For metapelites, P-T conditions of the M3 stage (Fig. 6b) were calculated using the Grt-Bt thermometer (Holdaway, 2000) and Grt-Al_2SiO_5-Pl-Qz (Holdaway, 2001) or Grt-Bt-Pl-Qz barometer (Wu et al., 2004). For metapsammite (15DG39), the Grt-Opx-Pl-

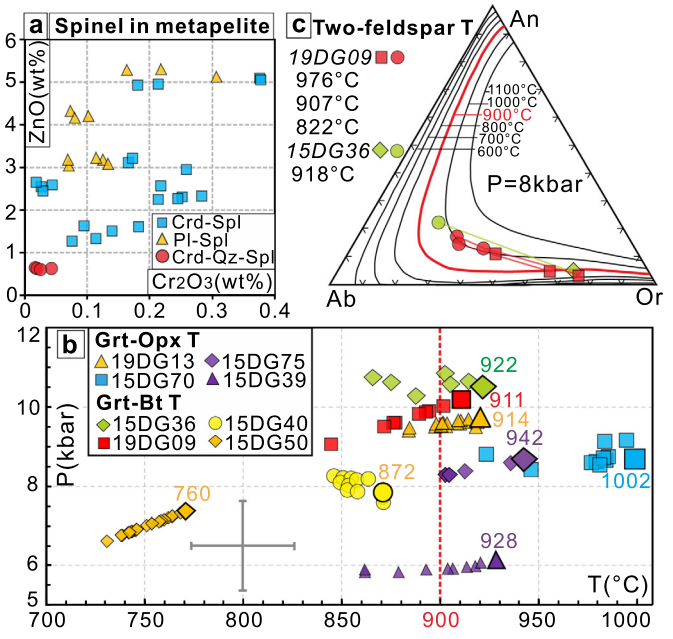

Fig. 6. Spinel compositions in metapelites and P-T conditions of the M3 stage. (**a**) Spinel in metapelite is grouped according to Crd-Spl, Pl-Spl and Crd-Qz+Spl intergrowth, and spinel in intergrowth with Crd-Qz symplectite are significantly lower in ZnO (0.6 wt%) and Cr_2O_3 (0.02–0.04 wt%). (**b**) Results of Fe-Mg exchange thermobarometry. Errors: Grt-Opx thermometer and Grt-Opx-Pl-Qz barometer, errors: ±50 °C, ±1.5 kbar; Grt-Bt thermometer, Grt-Al_2SiO_5-Pl-Qz or Grt-Bt-Pl-Qz barometer, errors: ±25 °C, ±1.2 kbar (shown as grey error bar). (**c**) Temperature results of two-feldspar thermometer using the calibration of Fuhrman and Lindsley (1988); detailed lamellae and host compositions and re-intergrated perthite/meso-perthite compositions can be found in Appendix C.5.

Qz thermobarometer (Lal, 2010) was used. Average compositions of homogeneous matrix plagioclase and biotite or orthopyroxene were used. Garnet compositions with lowest Fe# values were used for calculating the T_{max}. The calculated P-T conditions of samples 15DG36, 15DG39 and 19DG09 reached temperatures as high as 910–930 °C at varying pressures of ~6, ~10 and ~11 kbar (Fig. 6b). Samples 15DG50 and 15DG40 yield lower temperatures of 730–780 °C and 840–870 °C respectively, at pressures of 7–8 kbar. The results indicate that cordierite corona formed locally during decompression after peak-T conditions. Due to diffusion of Fe, Mg and Ti in biotite and orthopyroxene during cooling, the calculated temperatures spread to lower values (Fig. 6b). The obtained highest values are more approaching the temperatures the rocks have undergone. Therefore, the minimum temperatures during the M3 stage should be 910–930 °C.

For each single grain, mesoperthite/perthite compositions were reintegrated based on the areal proportions, and measured lamellae and host compositions. Lamellae areal proportions were measured from the BSE images, which occupy 14.5 vol% in sample 15DG36 and 51.6–63.5 vol% in sample 19DG09. Temperatures were calculated by two-feldspar thermometer using the calibration of Fuhrman and Lindsley (1988). The results are 976 °C, 918 °C, 907 °C and 822 °C (Fig. 6c), confirming the ultrahigh temperature (UHT) temperatures obtained above.

5. Geochronology

5.1. Zircon and titanite U-Pb ages (eclogites)

Zircon grains from eclogite samples 15DG70, 15DG75 and 15DG97 are roundish and present a core–rim or unzoned structure (Fig. 7a–c). Most cores are bright in CL, whereas the rims or unzoned grains are grey, some of which show a weak sector zoning. Most bright cores yield Miocene dates that are identical to the rims or unzoned grains, but one core analysis for sample 15DG97 yielded an older date of 1720 ± 28 Ma. Most analyses define similar mean $^{238}U/^{206}Pb$ ages of 15.7 ± 0.2 Ma (15DG70), 15.5 ± 0.3 Ma (15DG75) and 16.0 ± 0.2 Ma (15DG97). The Miocene zircons show variable HREE contents and no anomaly in Eu. The inherited core yields higher HREE and display a weak negative anomaly in Eu (Fig. 7d).

Titanite in samples 15DG70 and 15DG75 are unzoned in BSE; the grains are 80–150 µm in diameter (Fig. 7e–f) and have uranium contents of 80–400 ppm. The fraction of common Pb is high (40–95%) and the knowledge of the initial $^{207}Pb/^{206}Pb$ ratio is required to apply a common-lead correction. Therefore, lower intercept ages were obtained in the Tera-Wasserburg diagram by fitting isochrons. Each of them represents a binary mixing line between a common lead and a radiogenic lead component. Titanite lower-intercept $^{238}U/^{206}Pb$ ages are 14.3 ± 0.8 Ma (15DG70) and 12.8 ± 3.4 Ma (15DG75).

5.2. Monazite U-Th-Pb ages (metapelites)

Two migmatites (samples 15DG66 and 15DG74) from the country rock were investigated. In situ monazite dating was performed on thin sections to correlate ages with micro-textural positions. A total of 107 analyses were performed on monazite from four thin sections within which 21 analyses were excluded due to contamination of inclusions, not enough duration of signal or mixed ages (jump of $^{208}Pb/^{232}Th$ ratio during acquirement).

Monazites in sample 15DG66 are unzoned or have weak core-rim structure in the BSE-emission and commonly have diameter of 25–100 µm (Fig. 8a–c). Most monazites are included in biotite, plagioclase, quartz, K-feldspar or polyphase of the above minerals that present an embayment structure and represent crystallized melt (Fig. 8a–c). The monazite dates scatter between 25–20 Ma (Fig. 8f), with an older group at 26–22.5 Ma (N=35) and a younger group at 21.2 ± 0.7 Ma (N=5). The Y content is low (<3000 ppm) for the grains having the older dates and higher (up to 9000 ppm) for grains with younger dates. Monazite in sample 15DG74 shows variable zoning pattern of core-(mantle)-rim structure, patchy or unzoned with diameters of 30–100 µm (Fig. 8d,e). Most monazite grains are included in biotite, sillimanite or in retrograde anhedral muscovite forming fine-grained symplectite together with quartz (Fig. 8d,e). The dates scatter between 22 and 15 Ma (Fig. 8g) and are interpreted as two clusters with ages of 21.5–17 Ma (N 21) and 15.0 ± 0.4 Ma (N 9). A few grains yielded older dates of 445–132 Ma suggesting partial resetting or mixed analysis. From older dates to younger dates, yttrium contents show an increasing trend from 1000 to 15000 ppm.

Except for the two samples investigated here, published monazite and zircon trace elements and U-Th-Pb ages of metapelites from the same region (Wang et al., 2017b) are summarized in Fig. 8h–k. The calculated distribution coefficients (D_{REE}) with garnet shows that ~ 30 Ma zircon and monazite in metapelite are generally concordant with literatures for amphibolite-facies and granulite-facies metamorphism (Fig. 8h,i), indicating that ~30 Ma zircon and monazite formed in equilibrium with garnet during prograde growth. The summary of U-Th-Pb shows a metamorphic timescale from ~32 Ma to ~15 Ma with four peaks (Fig. 8j,k). The peaks at ~30 and ~24 Ma are based on more dates from single sample 15DG66 (81 analyses) and sample 15DG36 (Monazite 141 analyses, zircon 34 analyses), and dates from many more samples constitute the peaks at ~20 Ma and ~15 Ma (eight samples). Yttrium content in monazite is generally similar within 1000–10000 ppm for monazite with dates from ~32 Ma to 17 Ma, but shows an increase up to 25000~30000 ppm for the younger dates between 17 and 14 Ma. Nanogranite inclusions of Kfs-Qz-Ms were observed

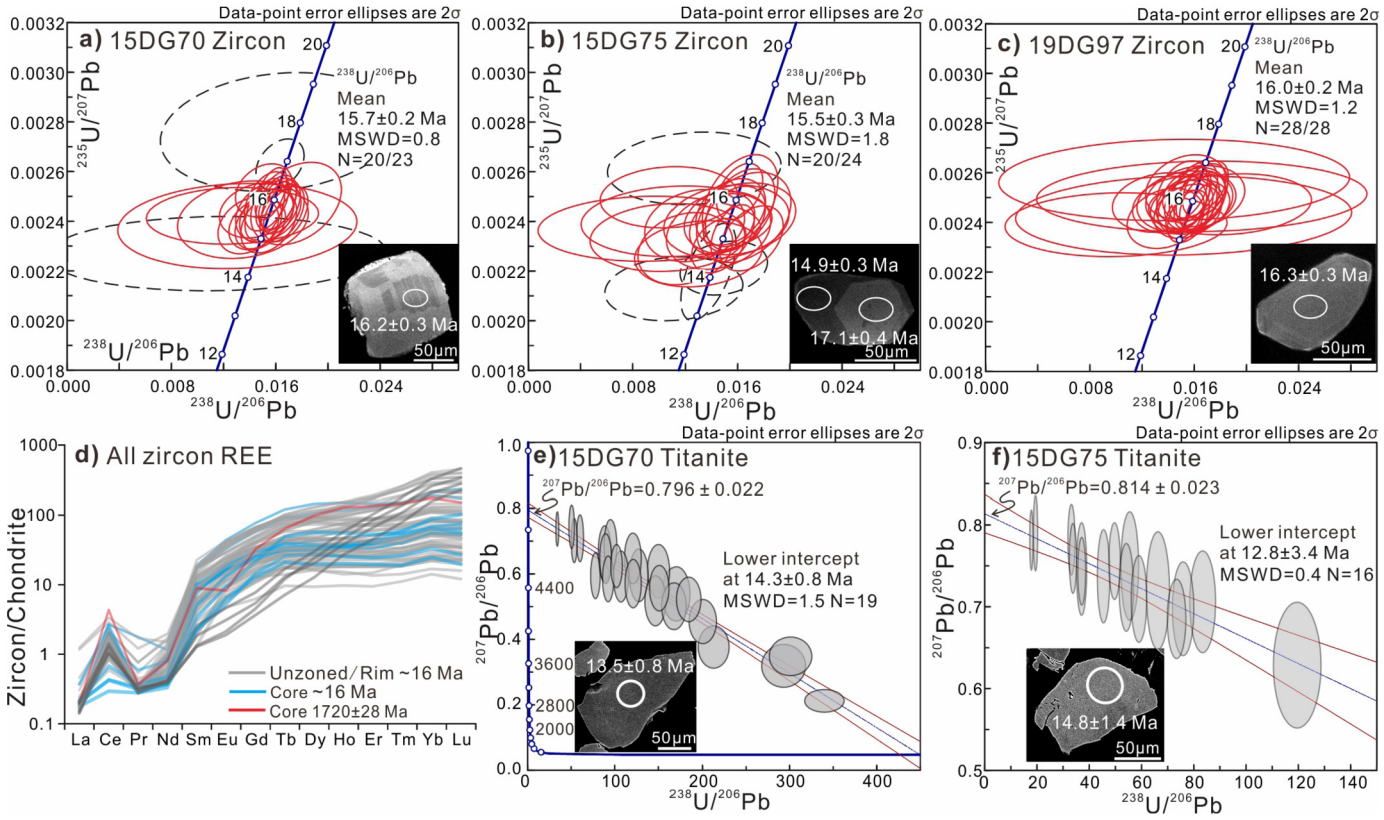

Fig. 7. U-Pb ages of zircon and titanite from eclogites. **a-d**) Cathodoluminescence images, U-Pb ages and REE pattern of zircon; Mean ages of zircons are $^{238}U/^{206}Pb$ ages; Dashed ellipses are dismissed from calculating weighted mean ages. **e-f**) Backscattered electronic images and U-Pb ages of titanite; The corresponding initial $^{207}Pb/^{206}Pb$ ratios for titanite are 0.796 ± 0.022 and 0.814 ± 0.023. The white circles represent an ion beam spot of 20–30 μm for zircon and a laser spot size of ~48 μm for titanite.

as early as ~31 Ma and sillimanite inclusions firstly appear within ~21 Ma monazite grain.

6. Discussion

6.1. P-T evolution of the central Himalayan eclogites

Recovering the P-T-t conditions of retrogressed eclogite is a puzzle as most of the eclogitic minerals (>95 vol%) were destabilized or re-equilibrated by intra-granular diffusion during UHT metamorphism. Phase equilibrium modelling associated with compositional isoplethes of observed and recovered omphacite and Zr-in-Rutile thermometry together provide conditions for the pressure peak (M1-stage) of 730–770 °C and ~20 kbar in the phengite stability field (grt+phe+omp+qz+rt), confirming previous interpretation that phengite was present at the pressure-peak (Groppo et al., 2007). Previous peak-pressure results of 20–21 kbar were based on the Garnet-Clinopyroxene equilibrium despite the use of phase diagrams (Wang et al., 2017a). However, this approach cannot be applied for our samples as HP garnet composition is no longer preserved and was modified by diffusion at the subsequent M2 and M3 stage. The Grt-Cpx-Pl-Qz barometer can only be used for the granulite-facies assemblage because garnet, clinopyroxene and plagioclase have not coexisted in equilibrium at the eclogitic M1 stage. Although similar pressure conditions were obtained for the M1-stage, the results presented here are based on mineral compositions (major and trace elements) that survived the UHT overprinting.

For the M3-stage, a UHT stage at 900–930 °C and <8 kbar was constrained by phase equilibrium modelling combined with peak-T mineral assemblage and plagioclase isopleths of Opx-Pl symplectite. Additional P-T estimates (900–970 °C, 6–11 kbar) in the migmatitic paragneiss were obtained using the Grt-Bt and GASP (GBPQ) thermobarometer, two-feldspar thermometer and Grt-Opx-Pl-Qz thermobarometer, confirming the UHT conditions. Although the observed spinel in equilibrium with Crd-Qz symplectites is suggestive but not diagnostic for UHT conditions, such an assemblage is commonly reported in UHT metapelites, whereas diagnostic mineral assemblages (e.g. Spr+Qz, Opx+Sil, osumilite) only occur in Mg-Al rich pelites that are rare in nature (Harley, 2008; Kelsey and Hand, 2015). Low Zn and Cr contents (Fig. 6a) in spinel and rutile exsolutions in biotite (Fig. 4d–i) suggest that these samples underwent extremely high temperatures (Harley, 1998). Biotite can be stable at temperatures over 900 °C (Kelsey and Hand, 2015), however, peak Fe-Mg contents in garnet and biotite are easily disturbed by diffusion during retrograde cooling. Zirconium contents in rutile formed at eclogite-facies conditions were not reset during the UHT stages so that rutile cannot be used to retrieve the highest temperatures experienced by these rocks (780–830 °C).

Combining the P-T conditions obtained for the M1, M2 and M3 stages of eclogite lenses and country rocks, the trajectory consists of HP eclogite-facies metamorphism followed by UHT granulite-facies metamorphism associated to a temperature increase of 100–200 °C. Although this result confirms the heating and decompression path for the central Himalayan eclogite (Ama Drime in Fig. 9, Groppo et al., 2007), it suggests that the degree of heating was much stronger than previously recognized. Granulitized eclogites and spinel-cordierite-bearing metapelites assembly were also observed from Sikkim and Eastern Himalayan Syntaxis, which represent the deepest portion along the strike of the Himalaya and are perhaps potential localities to examine UHT conditions within the over-thickened collisional belt.

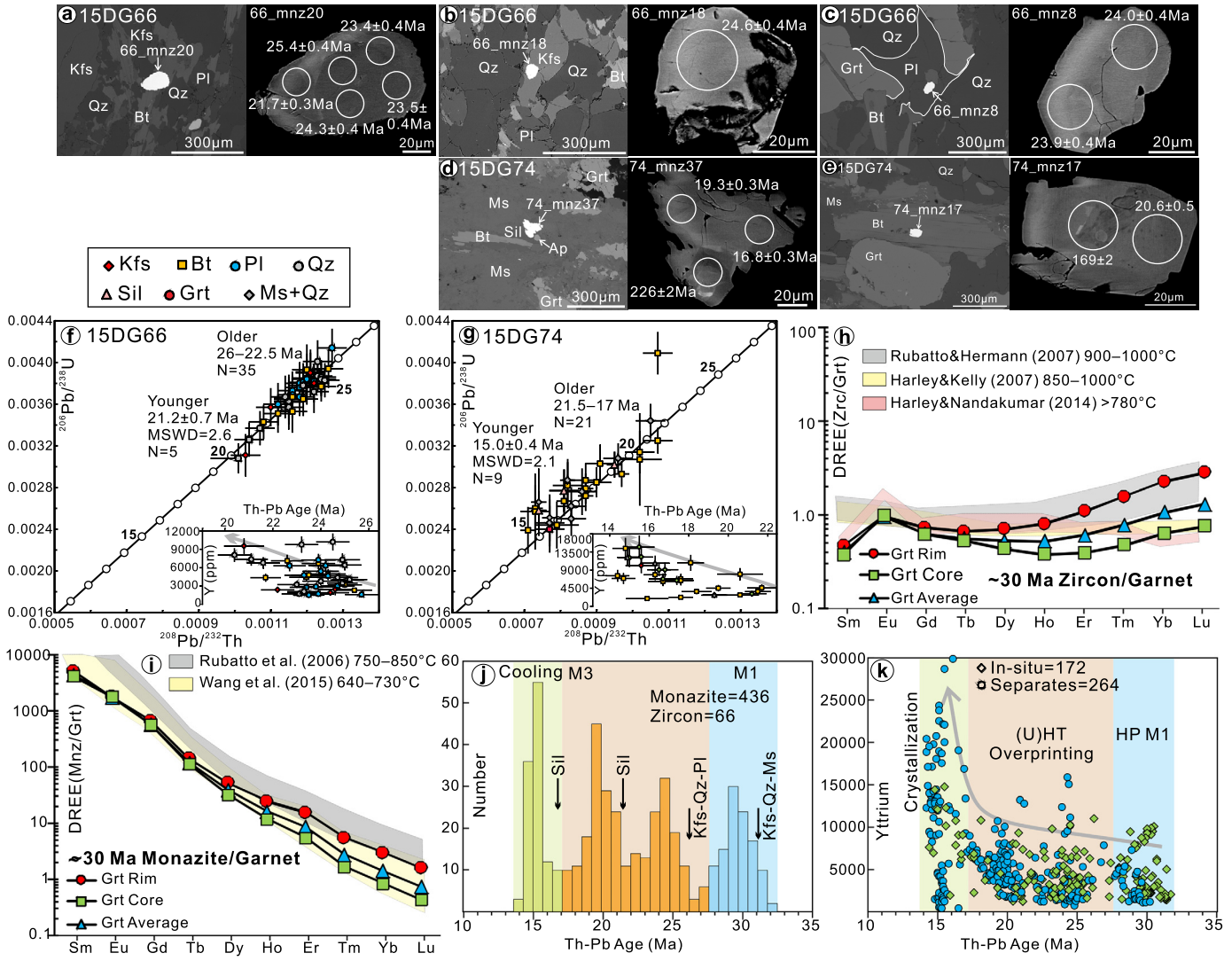

Fig. 8. Monazite textures, U-Th-Pb ages and summarized age results of metapelites from the country rock. **a-e**) Backscattered electronic images showing textural relationship between monazite and index minerals; **f-g**) Monazite U-Th-Pb age plots of samples from this study; **h-i**) Calculated distribution coefficients of REE between zircon or monazite and garnet. Only zircon and monazite dated to be ~30 Ma were used for calculation. Rim, core and average refer to the garnet portions for averaging the compositions. Trace elements of monazite and zircon are from Wang et al. (2017b) **j-k**) Summary of monazite U-Th-Pb ages, textures and yttrium contents from this study and Wang et al. (2017b), and result interpretation for linking the successive age populations to different metamorphic stages. The white circles represent a laser spot size of ~24 μm. References in the figures were listed in Appendix A.

6.2. Petrochronology of eclogitization and granulitization

Although most previous studies reported similar ages of 16–14 Ma in retrogressed eclogite from Everest east, Kharta, Sikkim and Bhutan, it is still largely debated whether these ages represent timing of eclogitization (Grujic et al., 2011; Wang et al., 2017a) or granulitization (Kellett et al., 2014). Apart from re-evaluating zircon U-Pb ages, textures and trace elements, our study provides titanite U-Pb ages of two eclogite samples and monazite Th-Pb ages of two migmatites from the country rocks. We propose that zircon and titanite U-Pb ages (16–14 Ma) from the eclogites, and monazite Th-Pb ages (20–15 Ma) in metapelites all record the timing of the UHT stage and subsequent cooling. This interpretation is based on the following observations: **i**) Some zircon show representative granulite-facies characteristics (Vavra et al., 1999) of sector zoning or fir leaves type in CL images (Fig. 7a,c); **ii**) Closure temperature of U-Pb system in titanite (600–700 °C) is lower than the recorded maximum temperatures (900–970 °C); **iii**) In sample 15DG66, monazite intergrowth with K-feldspar and in-situ crystallized melt and increasing Y and Eu anomaly through time suggest these monazite (25–22 Ma) were re-crystallized during high-temperature metamorphism associated with garnet breakdown and feldspar growth (Kohn, 2016); **iv**) In sample 15DG74, monazite grains showing 21.5–19 Ma ages are included in sillimanite and numerous sillimanite inclusions were observed in monazite with 21–20 Ma or ~15 Ma ages (Fig. 8d, Wang et al., 2017b); **v**) Monazite in a leucogranite dyke which cross-cuts the eclogite was dated at ~14 Ma (Wang et al., 2017b), reflecting crystallization during cooling.

Previous interpretation for an eclogitization timing at 16–14 Ma has to be reconsidered because: **i**) The flat HREE pattern in zircon was interpreted as the result of simultaneous growth with garnet during pressure peak (e.g. Grujic et al., 2011; Wang et al., 2017a). However, even newly crystallized zircons during overprinting would have much lower HREE than the protolith zircons, because protolith rocks are garnet-absent whereas garnet is still preserved at the peak-T or cooling due to incomplete reaction (Fig. 2g,h); **ii**) A number of rims show enrichment in HREE and are depleted in MREE (Fig. 7d), which suggests that at least these rims (~16 Ma) formed during/after garnet breakdown through decom-

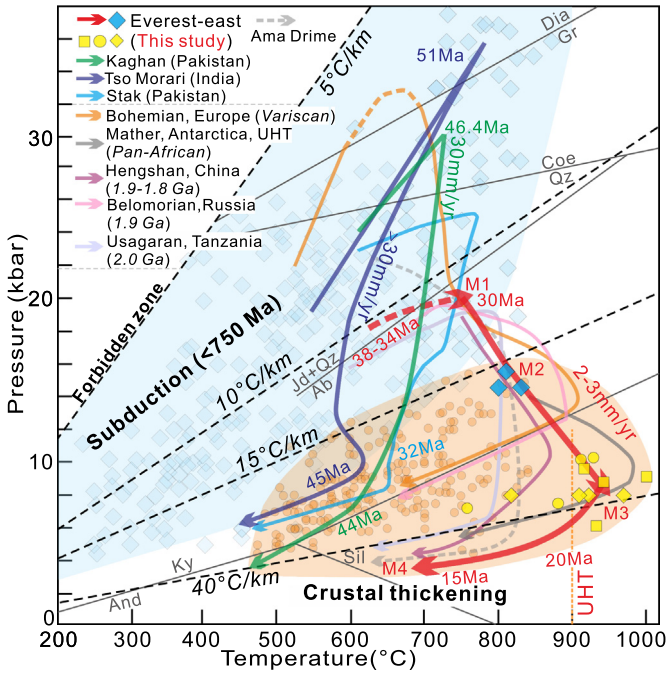

Fig. 9. Comparison of the pressure-temperature-time paths of Central and Western Himalayan eclogites, Paleoproterozoic eclogites and other HP-(U)HT rocks on Earth. P-T paths and ages: Ama Drime, Groppo et al. (2007); Pakistan and Tso Morati eclogite, Guillot et al. (2008), Lanari et al. (2013), Kouketsu et al. (2016); Bohemian Massif, Jedlicka and Faryad (2017); Mather Peninsula in East Antarctica, Harley (2008) and references therein; Hengshan, North China Craton, Zhao et al. (2001); Russian Belomorian, Imayama et al. (2017), Liu et al. (2017); Tanzanian Usagaran, Möller et al. (1995). Blue diamonds and domain are peak pressure-temperature conditions of subduction zones rocks younger than 750 Ma (Penniston-Dorland et al., 2015). Orange dots and domain are pressure-temperature conditions of Barrovian metamorphic rocks from the Himalayan collisional belt (Kohn, 2014). Blue diamonds, Grt-Cpx-Pl-Qz thermobarometer; yellow circles, Grt-Bt thermometer; yellow diamonds, two-feldspar thermometer; yellow squares, Grt-Opx thermometer.

pression; **iii**) Some suggest timing of eclogitization based on omphacite inclusion observed in the zircon rims (Wang et al., 2017a), but this can also simply indicate that zircon rims post-date the omphacite; zircon grew during burial metamorphism and, in case of resetting during granulitization, could also have preserved omphacite inclusions.

If zircon in the eclogite only records the timing of cooling after granulitization, then what is the timing of eclogitization? The study of the country rock suggests that the timing of high-pressure metamorphism was occasionally recorded by monazite and zircon in some of the metapelites that were isolated from partial melt domains. In our previous work (Wang et al., 2017b), most metapelites from the same region only record the timing of UHT resetting or crystallization cooling at 20–15 Ma (Fig. 8j,k); In only one sample, monazite and zircon show a large cluster of older ages at ~30 Ma, which represent the timing of high-pressure metamorphism, as supported by consistent D_{REE}(Zrc/Grt) or D_{REE}(Mnz/Grt) with literature data (Fig. 8h,i) indicating equilibrium with prograde garnet (Y-decreasing growth zoning) and polyphase melt inclusions of Kfs-Ms-Qz in monazite indicating prograde melting (Fig. 8j). The timing of high-pressure metamorphism in Everest east is coherent with that obtained in the upper GHC along the Himalayan strike (32–27 Ma, e.g. Imayama et al., 2012). Therefore, we suggest that timing of eclogitization is around ~30 Ma. Timing of eclogitization is absent in the eclogite zircons due to strong Miocene overprinting. Garnet Lu-Hf ages of 38–34 Ma from the ADM eclogites (Kellett et al., 2014) are probably older than the HP event as it suffers from a series of problems to shift the extracted Lu-Hf data toward older ages (see summary in Webb et al., 2017). Conclusively, the Indian felsic crust (GHC) in the central portion underwent eclogitization (~70 km) during~30 Ma and were overprinted by UHT conditions at middle crust (20–40 km) during 20–15 Ma.

6.3. How to form two contrasting eclogite types in the Himalaya?

The existence of two contrasting eclogite types in the Himalaya was proposed since the first discovery of granulitized eclogites in the central Himalaya (CHE, Lombardo and Rolfo, 2000), to distinguish them from the coesite-bearing ultrahigh pressure (UHP) eclogite from western Himalaya (WHE, O'Brien et al., 2001; Guillot et al., 2008). Their differences are renewed according to the new P-T-t path (Fig. 9) and listed below: **i**) The CHE crop out in the highly metamorphosed orogenic core that is ~100 km south to the Indus-Zangpo suture zone and can be extended for ~2400 km along strike; the WHE form isolated UHP domes close to the suture zone, that is in contact with superficial or shallowly buried ophiolite/melange; **ii**) Geothermal gradient of the peak-pressure stage for the CHE (11.5 ±1.5 °C/km, Fig. 9) is warmer whereas the WHE is colder (6–8 °C/km, Guillot et al., 2008) than a typical Phanerozoic cold subduction thermal-gradient of <10 °C/km (Brown, 2006); **iii**) The CHE underwent heating and decompression from peak-P to peak-T (△T 100–200 °C) and were highly overprinted by UHT conditions during exhumation, whereas the WHE underwent cooling or near-isothermal decompression (Lanari et al., 2013); i**v**) The timing of eclogitization in the CHE largely postdates (△t 25–20 Myr) whereas WHE is nearly simultaneous (△t 10–5 Myr, Donaldson et al., 2013) from the timing of initial collision (59 ±1 Ma, Hu et al., 2015); **v**) The duration of exhumation to middle crust in the CHE lasts much longer (△t ~20 Myr) and slower (2–3 mm/yr) compared to WHE (△t ~2 Myr, ~30 mm/yr, Donaldson et al., 2013); **vi**) The CHE were buried during the mature collisional stage and surrounded by an over-thickened felsic lower crust (~60 km) that has similar density (~2.8) as their host paragneiss/granite (Gao et al., 2016); whereas the WHE were buried during the infant collisional stage when the Himalayan lower crust was thin (~33 km) and surrounded by lithospheric mantle (density 3.3).

The above renewed distinctions allow us to summarize key tectonic processes from infant to mature collisional stages. It is commonly supposed that the WHE were rapidly exhumed to the middle crust by break-off of the Neo-Tethyan oceanic slab (Kohn and Parkinson, 2002). However, the break-off would cause slab pull, the dominant driving force for plate motion, to stop (Conrad and Lithgow-Bertelloni, 2004), whereas the Indian continent was continuously subducted till present. This break-off model is also in contradiction with the two-stage eclogite exhumation in northwest Pakistan Himalaya (Kaghan and Stak in Fig. 9). A diachronous slab detachment model was proposed to interpret the timing of south-Tibet volcanism and metamorphism (Webb et al., 2017), but it requires a mid-Miocene timing of eclogitization in CHE that is not supported by our results. Some studies suggested a steep subduction in western Himalaya and a flat subduction in central and eastern Himalaya to explain the contrasting P-T of the eclogites (e.g. Guillot et al., 2008). However, such a model is not in line with the present geophysical seismic observations of a steep subduction in central and eastern Himalaya and a flat subduction in western Himalaya (Liang et al., 2016). Therefore, this model needs a subduction angle change that lack support from mantle-derived magmatic evidence. On the contrary, a heavy overprinting and similar timing of eclogitization of the Stak eclogite (Lanari et al., 2013) as the CHE suggest that the central and western Himalaya should share similar tectonic process during Oligocene.

Here, we proposed a simpler model (Fig. 10a,b) compatible with both a stable driving force without need of slab break-off and the seismic observations suggesting a constant slab geometry along the belt. **i**) During the infant collisional stage (early

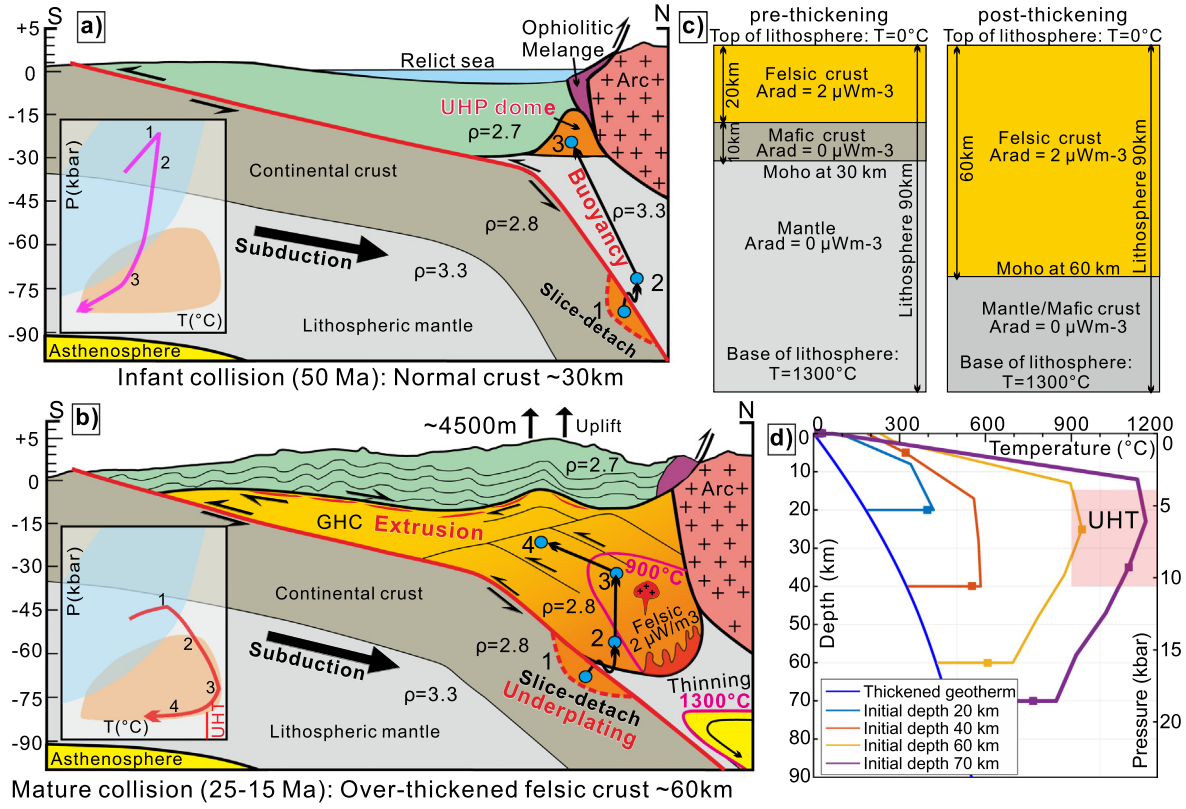

Fig. 10. Model illustrating the formation of Himalayan eclogites and UHT conditions. **a,b**) Formation of two contrasting types of eclogite due to different crustal thickness and topography in different collisional stages. During the infant collisional stage, the crust was thin and cold eclogites were exhumed rapidly by buoyancy without strong overprinting. During the mature collisional stage, the crust was over-thickened and granulitized eclogites were exhumed by underplating and tectonic extrusion. At this stage, a combined heat source of overthickened felsic lower crust and thinning of lithosphere may have contributed to the generation of UHT conditions in the middle and lower crust. **c,d**)1-D thermal model for instantaneous triple crustal thickening of the felsic crust to ~60 km and thinning of the lithosphere to ~90 km. The modelling generally follows the setup and code of Gerya and Stöckhert (2006) and Clark et al. (2011) but parameters were changed to be in line with the Himalayan observations: P-T-t paths/curve are results from duration of uplift by 30 Myr, amount of uplift by 70 km and delay by 25 Myr after initial collision. A latent heat of melting (320 kJ kg^{-1}) was included. Note that UHT conditions at middle crust could be achieved 30–40 Myr after thickening for rocks buried to >60 km.

Eocene), the Himalayan crust was thin (~30 km) and elevation of the suture zone region was below sea level (relic sea basin). Therefore, the density contrast between host paragneiss/granite (density 2.8 g cm^{-3}) of the UHP eclogite and the surrounding lithospheric mantle (density 3.3 g cm^{-3}) was large enough to generate buoyancy force and rapidly bring these rocks up to the middle crust level. Therefore, these eclogites underwent a near-vertical exhumation along the subduction interface and record an isothermal/cooling decompression associated to rapid exhumation (~30 mm/yr). **ii**) During the mature collisional stage (Oligocene-Miocene, Fig. 10b), the subducted continental crust was continuously detached as slices and stacked at the base of the orogenic root (Gao et al., 2016). After 30–20 Myr of stacking, the orogenic crust was over-thickened (55–65 km thick) with sediments/granite. Due to over-thickening, there was not much density difference between the newly detached eclogite-bearing felsic slices (mainly paragneiss/granite, density 2.8 g cm^{-3}) and the over-thickened orogenic root (density 2.8 g cm^{-3}). Therefore, exhumation of the HP units was controlled by underplating which is much slower than the buoyancy-driven mechanism. At this stage, UHT conditions at middle-lower crust cause granulite-facies metamorphism, largely resetting mineral ages and compositions from the high-pressure stage. Finally, when enough strain was accumulated to cause crustal failure, movement along large-scale thrusts (e.g. MCT) and passive-roof faults (e.g. STD) caused lateral tectonic extrusion of these rocks (Burchfiel et al., 1992), so that they mostly crop out today in the collisional metamorphic core, much southern to the suture zone.

Although UHT rocks are widespread across Precambrian and Phanerozoic metamorphic belts, the heat source is still controversial—how can continental crust reach such extreme conditions (Clark et al., 2011)? The Himalaya is a prototype of large and hot collisional orogen and UHT conditions at its present-day middle crust has been predicted by numerical modelling (Jamieson et al., 2004), but metamorphic evidence of UHT records was still missing. Our results provide pieces of evidence—both textural and thermobarometric—for UHT conditions of 900–970 °C that occurred at middle-lower crustal depth (20–40 km) overprinting the mineral record of a previous eclogite-facies stage through a heating and decompression path. Such a path resembles very much to the UHT-ITD path defined by the kyanite-bearing UHT granulites from East Antarctica (Fig. 9, Harley (2008) and references therein). Taking into account the crustal architecture of the Himalaya and Tibetan Plateau, UHT conditions in the Himalaya were probably caused by a combined effect of radioactive heating by Th, U and K elements in felsic crust (Clark et al., 2011) and thinning of lithosphere. To support this, we re-ran a 1-D thermal model by changing the parameters to fit Himalayan observations. The results indicate that UHT condition could be easily produced by a combined effect of thickened radioactive felsic crust to ~60 km and thinning of lithosphere to <90 km (Fig. 10c,d). It also indicates that UHT conditions could be achieved 30–40 Myr after thickening for rocks buried to >60 km. This is consistent with our petrochronological dataset, which suggests that UHT condition were reached 35–40 Myr after the initial collision since 59±1 Ma (Hu et al., 2015), much earlier than previously modelled (>50 Myr, Jamieson et al., 2004; Clark et al., 2011). However, by using normal

radioactivity parameter of 2 $\mu W/m^3$, neither cumulated radioactive heat of an over-thickened felsic crust of ~60 km, nor thinning of lithosphere to ~90 km alone can produce UHT condition at middle-lower crust (Appendix B.5). The modelling is in line with geological evidences: **1**) Radioactive heating is possible as the Himalayan lower crust made of sediments and granite was stacked to a pile of 55~65 km thick since ~30 Ma according to this study and seismic profile of Gao et al. (2016); **2**) Thinning of the lithosphere is supported by observations indicating that the thickened lower crust in southern Tibet underwent partial melting with significant contributions from juvenile magma from Oligocene to Miocene (Ji et al., 2020). In conclusion, the UHT conditions obtained in this study are the highest temperature ever reported within the Himalaya and they allow us to better understand the heat source and timescale of UHT condition during continental collision, such as those from East Antarctica.

6.4. Implications for collisional tectonics on early Earth

By dissecting the formation of two contrasting eclogite types in the Himalaya, it is now clear that: during continental collision, cold eclogites are more easily exhumed during the early infant collisional stage when the crustal thickness of the subducting front is normal or even shallower than 30 km (negative topography); whereas granulitized eclogites will be exhumed during the relatively-late and mature collisional stage, when the orogenic crust is over-thickened (>60 km). This implies that: 1) most cold eclogites will be denudated or eroded much faster because they were exhumed earlier and sits on a more superficial level; 2) although (cold) eclogites are continuously being produced through deep subduction during the mature collision stage, these eclogites will not be easily exhumed and instead will be stacked into the orogenic felsic lower crust to undergo long-lived (>20–15 Myr) high-temperature overprinting; 3) in mature collisional belts like the Himalaya, the middle-lower crust reached high to ultrahigh temperature conditions promoting intense overprinting; such an extremely high to ultrahigh temperature pattern is perhaps more common than previously recognized and represents a feature of mature continental collision. For example, HP eclogites were also overprinted by HT-UHT event through heating and decompression paths in the Variscan Bohemian Massif or Paleoproterozoic Belomorian (Fig. 9). Nevertheless, there exist collisional belts for which continental collision does not result in a dramatic overprinting (such as the Alpine orogeny)—if the lower crust of the subducting plate is not so over-thickened, cold eclogites are better preserved.

This model may provide an explanation why eclogites are rarely preserved in Earth's primitive metamorphic terranes. Although previous studies suggested a Paleoproterozoic/Archean subduction based on the oldest eclogites, it is uncertain whether the subduction was oceanic (Mints et al., 2014) or continental (Weller and St-Onge, 2017), and what kind of tectonic regime caused their subsequent granulitization. Compared with the central Himalayan eclogites, the oldest (granulitized) eclogites on earth (Fig. 9), such as those from Russian Belomorian (~1.90 Ga, Imayama et al., 2017), Tanzanian Usagarian (~2.0 Ga, Möller et al., 1995) and Canadian Trans-Hudson (~1.83 Ga, Weller and St-Onge, 2017), share similarities in slow exhumation rates (<5 mm/yr), prolonged exhumation (>15–20 Myr) and extreme HT-UHT overprinting. These Paleoproterozoic eclogites most likely represent the exhumed over-thickened lower crust after a mature continental collision similar to what happened in the Himalaya. In other words, the oldest known (granulitized) eclogites on Earth should have undergone a Himalayan-type continental subduction/collision around 2.0–1.8 Ga. Because localities of the Paleoproterozoic granulitized eclogites were scattered in different belts on earth (Fig. 9 and Appendix B.6), we suggest that Himalaya-type continental subduction/collision should have become a global pattern during the Paleoproterozoic era (2.0–1.8 Ga), which is probably related to the assembly of Nuna Supercontinent (Wan et al., 2020). Collisional orogeny perhaps have initiated in some local regions during late-Archean and the mystery lies within the medium- to high-pressure granulites (Appendix B.7), which is the dominate rocks in the Himalayan metamorphic core or other Phanerozoic collisional belts on Earth.

7. Conclusions

1) The central Himalayan eclogites underwent eclogitization at conditions of 730–770 °C and ~20 kbar (~11 °C/km) around 30 Ma, and were overprinted during 25–15 Ma to UHT conditions of 900–970 °C and 6–11 kbar, indicating a heating and decompression path with slow exhumation rate (2–3 mm/yr) and prolonged time (10–15 Myr) at (U)HT conditions.

2) UHT metamorphism is reported for the first time in the Himalayan belt, which was induced by combined effects of over-thickened (~60 km) radioactive felsic crust and thinning of lithosphere to <90 km.

3) Formation of cold vs. granulitized eclogites during the Himalayan orogeny are caused by their exhumation that occurred during different collisional stages (infant vs. mature) involving different crustal thickness (normal ~30 km vs. over-thickened ~60 km).

4) We propose that the oldest eclogites on Earth were intensively overprinted because they were stacked to the over-thickened orogenic crust during a Himalaya-type continental subduction/collision, which should have become a global pattern during the Paleoproterozoic (2.0–1.8 Ga).

CRediT authorship contribution statement

Jia-Min Wang: Conceptualization, Funding acquisition, Investigation, Methodology, Writing – original draft. **Pierre Lanari:** Conceptualization, Methodology, Writing – review & editing. **Fu-Yuan Wu:** Funding acquisition, Supervision. **Jin-Jiang Zhang:** Funding acquisition, Supervision. **Gautam Prashad Khanal:** Investigation. **Lei Yang:** Investigation.

Declaration of competing interest

The authors declare that they have no known competing financial interests or personal relationships that could have appeared to influence the work reported in this paper.

Acknowledgements

Discussions with D. Rubatto, J. Hermann, C. Clark, J.H. Guo, C.J. Wei, B. Wan, B. Zhang and S.J. Jiao inspired the authors. The authors thank Q.L. Li, X.X. Lin, J. Li, Y.H. Yang and Q. Mao for analytical help. We are grateful to our driver Dorji, who supported our group with field work in Tibet for >20 years. Constructive reviews by S.L. Harley and T. Imayama greatly improved the manuscript. This work was supported by the National Natural Science Foundation of China (grant numbers 41888101 and 41972065) and the Second Tibetan Plateau Scientific Expedition and Research program (2019QZKK0703).

Appendix A. Supplementary material

Supplementary material related to this article can be found online at https://doi.org/10.1016/j.epsl.2021.116760.

References

Brown, M., 2006. Duality of thermal regimes is the distinctive characteristic of plate tectonics since the Neoarchean. Geology 34, 961–964.

Burchfiel, B.C., Zhiliang, C., Hodges, K.V., Yuping, L., Royden, L.H., Changrong, D., Jiene, X., 1992. The South Tibetan detachment system, Himalayan Orogen: extension contemporaneous with and parallel to shortening in a collisional mountain belt. Spec. Pap., Geol. Soc. Am. 269, 1–41.

Clark, C., Fitzsimons, I.C.W., Healy, D., Harley, S.L., 2011. How does the continental crust get really hot? Elements 7, 235–240.

Condie, K.C., Kröner, A., 2008. When did plate tectonics begin? Evidence from the geologic record. Spec. Pap., Geol. Soc. Am. 440, 281–294.

Connolly, J.A.D., 2009. The geodynamic equation of state: what and how. Geochem. Geophys. Geosyst. 10, 10.

Conrad, C.P., Lithgow-Bertelloni, C., 2004. The temporal evolution of plate driving forces: importance of "slab suction" versus "slab pull" during the Cenozoic. J. Geophys. Res., Solid Earth 109.

Donaldson, D.G., Webb, A.A.G., Menold, C.A., Kylander-Clark, A.R.C., Hacker, B.R., 2013. Petrochronology of Himalayan ultrahigh-pressure eclogite. Geology 41, 835–838.

Eckert, J.O., Newton, R.C., Kleppa, O.J., 1991. The ΔH of reaction and recalibration of garnet-pyroxene-plagioclase-quartz geobarometers in the CMAS system by solution calorimetry. Am. Mineral. 76, 148–160.

Fuhrman, M.L., Lindsley, D.H., 1988. Ternary-feldspar modeling and thermometry. Am. Mineral. 73 (3–4), 201–215.

Gao, R., Lu, Z., Klemperer, S.L., Wang, H., Dong, S., Li, W., Li, H., 2016. Crustal-scale duplexing beneath the Yarlung Zangbo suture in the western Himalaya. Nat. Geosci. 9, 555.

Gerya, T., Stöckhert, B., 2006. Two-dimensional numerical modeling of tectonic and metamorphic histories at active continental margins. Int. J. Earth Sci. 95, 250–274.

Groppo, C., Lombardo, B., Rolfo, F., Pertusati, P., 2007. Clockwise exhumation path of granulitized eclogites from the Ama Drime range (Eastern Himalayas). J. Metamorph. Geol. 25, 51–75.

Grujic, D., Warren, C.J., Wooden, J.L., 2011. Rapid synconvergent exhumation of Miocene-aged lower orogenic crust in the eastern Himalaya. Lithosphere 3, 346–366.

Guillot, S., Mahéo, G., de Sigoyer, J., Hattori, K.H., Pêcher, A., 2008. Tethyan and Indian subduction viewed from the Himalayan high- to ultrahigh-pressure metamorphic rocks. Tectonophysics 451, 225–241.

Harley, S.L., 1998. On the occurrence and characterization of ultrahigh-temperature crustal metamorphism. Geol. Soc. (Lond.) Spec. Publ. 138, 81–107.

Harley, S.L., 2008. Refining the P-T records of UHT crustal metamorphism. J. Metamorph. Geol. 26, 125–154.

Holdaway, M.J., 2000. Application of new experimental and garnet Margules data to the garnet-biotite geothermometer. Am. Mineral., 881.

Holdaway, M.J., 2001. Recalibration of the GASP geobarometer in light of recent garnet and plagioclase activity models and versions of the garnet-biotite geothermometer. Am. Mineral., 1117.

Holland, T.J.B., Powell, R., 2011. An improved and extended internally consistent thermodynamic dataset for phases of petrological interest, involving a new equation of state for solids. J. Metamorph. Geol. 29, 333–383.

Hu, X., Garzanti, E., Moore, T., Raffi, I., 2015. Direct stratigraphic dating of India-Asia collision onset at the Selandian (middle Paleocene, 59 $\pm$ 1 Ma). Geology 43, 859–862.

Imayama, T., Oh, C.-W., Baltybaev, S.K., Park, C.-S., Yi, K., Jung, H., 2017. Paleoproterozoic high-pressure metamorphic history of the Salma eclogite on the Kola Peninsula, Russia. Lithosphere 9, 855–873.

Imayama, T., Takeshita, T., Yi, K., Cho, D.-L., Kitajima, K., Tsutsumi, Y., Kayama, M., Nishido, H., Okumura, T., Yagi, K., Itaya, T., Sano, Y., 2012. Two-stage partial melting and contrasting cooling history within the higher Himalayan crystalline sequence in the far-eastern Nepal Himalaya. Lithos 134–135, 1–22.

Jamieson, R.A., Beaumont, C., Medvedev, S., Nguyen, M.H., 2004. Crustal channel flows: 2. Numerical models with implications for metamorphism in the Himalayan-Tibetan orogen. J. Geophys. Res. 109.

Jedlicka, R., Faryad, S.W., 2017. Felsic granulite with layers of eclogite facies rocks in the Bohemian Massif; did they share a common metamorphic history? Lithos 286–287, 408–425.

Ji, W.-Q., Wu, F.-Y., Liu, X.-C., Liu, Z.-C., Zhang, C., Liu, T., Wang, J.-G., Paterson, S.R., 2020. Pervasive Miocene melting of thickened crust from the Lhasa terrane to Himalaya, southern Tibet and its constraint on generation of Himalayan leucogranite. Geochim. Cosmochim. Acta 278, 137–156.

Kellett, D.A., Cottle, J.M., Smit, M., 2014. Eocene deep crust at Ama Drime, Tibet: early evolution of the Himalayan orogen. Lithosphere 6, 220–229.

Kelsey, D.E., Hand, M., 2015. On ultrahigh temperature crustal metamorphism: phase equilibria, trace element thermometry, bulk composition, heat sources, timescales and tectonic settings. Geosci. Front. 6, 311–356.

Kohn, M.J., Parkinson, C.D., 2002. Petrologic case for Eocene slab breakoff during the Indo-Asian collision. Geology 30, 591–594.

Kohn, M.J., 2014. Himalayan metamorphism and its tectonic implications. Annu. Rev. Earth Planet. Sci. 42, 381–419.

Kouketsu, Y., Hattori, K., Guillot, S., Rayner, N., 2016. Eocene to Oligocene retrogression and recrystallization of the Stak eclogite in northwest Himalaya. Lithos 240–243, 155–166.

Lal, R.K., 2010. Internally consistent recalibrations of mineral equilibria for geothermobarometry involving garnet–orthopyroxene–plagioclase–quartz assemblages and their application to the South Indian granulites. J. Metamorph. Geol. 11, 855–866.

Lanari, P., Riel, N., Guillot, S., Vidal, O., Schwartz, S., Pecher, A., Hattori, K.H., 2013. Deciphering high-pressure metamorphism in collisional context using microprobe mapping methods: application to the Stak eclogitic massif (northwest Himalaya). Geology 41, 111–114.

Lanari, P., Vidal, O., De Andrade, V., Dubacq, B., Lewin, E., Grosch, E.G., Schwartz, S., 2014. XMapTools: a MATLAB©-based program for electron microprobe X-ray image processing and geothermobarometry. Comput. Geosci. 62, 227–240.

Le Fort, P., 1986. Metamorphism and magmatism during the Himalayan collision. Geol. Soc. (Lond.) Spec. Publ. 19, 159–172.

Li, Q., Zhang, L., Fu, B., Bader, T., Yu, H., 2019. Petrology and zircon U–Pb dating of well-preserved eclogites from the Thongmön area in central Himalaya and their tectonic implications. J. Metamorph. Geol. 37, 203–226.

Liang, X., Chen, Y., Tian, X., Chen, Y.J., Ni, J., Gallegos, A., Klemperer, S.L., Wang, M., Xu, T., Sun, C., Si, S., Lan, H., Teng, J., 2016. 3D imaging of subducting and fragmenting Indian continental lithosphere beneath southern and central Tibet using body-wave finite-frequency tomography. Earth Planet. Sci. Lett. 443, 162–175.

Liu, F., Zhang, L., Li, X., Slabunov, A.I., Wei, C., Bader, T., 2017. The metamorphic evolution of Paleoproterozoic eclogites in Kuru-Vaara, northern Belomorian Province, Russia: constraints from P-T pseudosections and zircon dating. Precambrian Res. 289, 31–47.

Lombardo, B., Rolfo, F., 2000. Two contrasting eclogite types in the Himalayas: implications for the Himalayan orogeny. J. Geodyn. 30, 37–60.

Mints, M.V., Belousova, E.A., Konilov, A.N., Natapov, L.M., Shchipansky, A.A., Griffin, W.L., O'Reilly, S.Y., Dokukina, K.A., Kaulina, T.V., 2010. Mesoarchean subduction processes: 2.87 Ga eclogites from the Kola Peninsula, Russia. Geology 38, 739–742.

Möller, A., Appel, P., Mezger, K., Schenk, V., 1995. Evidence for a 2 Ga subduction zone: eclogites in the Usagaran belt of Tanzania. Geology 23, 1067–1070.

Moyen, J.-F., Stevens, G., Kisters, A., 2006. Record of mid-Archaean subduction from metamorphism in the Barberton terrain, South Africa. Nature 442, 559–562.

O'Brien, P.J., Röhr, C., Okrusch, M., Patzak, M., 1992. Eclogite facies relics and a multistage breakdown in metabasites of the KTB pilot hole, NE Bavaria: implications for the Variscan tectonometamorphic evolution of the NW Bohemian Massif. Contrib. Mineral. Petrol. 112, 261–278.

O'Brien, P.J., Zotov, N., Law, R., Khan, M.A., Jan, M.Q., 2001. Coesite in Himalayan eclogite and implications for models of India-Asia collision. Geology 29, 435–438.

O'Brien, P.J., 2018. Eclogites and other high-pressure rocks in the Himalaya: a review. Geol. Soc. (Lond.) Spec. Publ. 483, SP483.413.

Penniston-Dorland, S.C., Kohn, M.J., Manning, C.E., 2015. The global range of subduction zone thermal structures from exhumed blueschists and eclogites: rocks are hotter than models. Earth Planet. Sci. Lett. 428, 243–254.

Vavra, G., Schmid, R., Gebauer, D., 1999. Internal morphology, habit and U-Th-Pb microanalysis of amphibolite-to-granulite facies zircons: geochronology of the Ivrea Zone (Southern Alps). Contrib. Mineral. Petrol. 134, 380–404.

Wang, Y., Zhang, L., Zhang, J., Wei, C., 2017a. The youngest eclogite in central Himalaya: P–T path, U–Pb zircon age and its tectonic implication. Gondwana Res. 41, 188–206.

Wang, J.-M., Wu, F.-Y., Rubatto, D., Liu, S.-R., Zhang, J.-J., Liu, X.-C., Yang, L., 2017b. Monazite behaviour during isothermal decompression in pelitic granulites: a case study from Dinggye, Tibetan Himalaya. Contrib. Mineral. Petrol. 172, 81.

Wan, B., Yang, X., Tian, X., Yuan, H., Kirscher, U., Mitchell, R.N., 2020. Seismological evidence for the earliest global subduction network at 2 Ga ago. Sci. Adv. 6, eabc5491.

Webb, A.A.G., Guo, H., Clift, P.D., Husson, L., Müller, T., Costantino, D., Yin, A., Xu, Z., Cao, H., Wang, Q., 2017. The Himalaya in 3D: slab dynamics controlled mountain building and monsoon intensification. Lithosphere 9, 637–651.

Weller, O.M., St-Onge, M.R., 2017. Record of modern-style plate tectonics in the Palaeoproterozoic Trans-Hudson orogen. Nat. Geosci. 10, 305–311.

Whitney, D.L., Evans, B.W., 2010. Abbreviations for names of rock-forming minerals. Am. Mineral. 95, 185–187.

Wu, C.-M., Zhang, J., Ren, L.-D., 2004. Empirical garnet-biotite-plagioclase-quartz (GBPQ) geobarometry in medium- to high-grade metapelites. J. Petrol. 45, 1907–1921.

Xu, C., Kynický, J., Song, W., Tao, R., Lü, Z., Li, Y., Yang, Y., Pohanka, M., Galiova, M.V., Zhang, L., Fei, Y., 2018. Cold deep subduction recorded by remnants of a Paleoproterozoic carbonated slab. Nat. Commun. 9, 2790.

Zhao, G., Cawood, P.A., Wilde, S.A., Lu, L., 2001. High-pressure granulites (retrograded eclogites) from the Hengshan Complex, North China craton: petrology and tectonic implications. J. Petrol. 42, 1141–1170.